

Color Facial Image Representation with New Quaternion Gradients

Artyom Grigoryan and Sos Agaian, Department of Electrical and Computer Engineering, The University of Texas at San Antonio, USA, Computer Science Department, College of Staten Island and the Graduate Center, Staten Island, NY, USA

Abstract

This paper proposes a new color image representation and multiple feature fusion based method for improving color face recognition performance under different lighting conditions. First, a new image color image representation has been derived. Second, a quaternion gradient has been given to enhance and extract the faces/object's edges, contours, and texture. Also, we propose a novel feature representation based on Quaternion Gradient-based LBP tool for color face recognition. Finally, we present a concept of combining the color facial recognition system, which is based on the local quaternion gradients based binary patterns LBP Image Representation, and a new color-to-gray new mapping. The presented concept can be used for surveillance, security systems, computer animation, face tagging, human-computer interface, biometric identification, behavioral analysis, content-based image and video indexing applications.

Introduction

The goal of face recognition (face verification and face identification) is to identify/verify automatically a person from a digital image or a video sequence in not controlled: environments (background, lighting conditions, camera distance, and thus the size and orientation of the head), image age or a video sequence age, camera use (light intensity, focal length, color balance, etc.) and gallery/database size. It should be noted that a face verification involves a one-to-one match that compares a query face image against a template face image whose identity is being claimed, and face identification involves one-to-many matches that compares a query face image against all the template images in the database, to determine the identity of the query face [1]-[9].

Face recognition (FR) has attracted a lot of attention recently due to a) the huge number of applications both in the commercial and government sectors, such as surveillance, security systems, computer animation, face tagging, human-computer interface, biometric identification, behavioral analysis, content-based image and video indexing; b) big advantages over other biometric knowhow: easy to use, nonintrusive, and it is a natural process (because human can do it without much conscious).

Recently, several face recognition systems have been developed including LBP method which is one of the most powerful, simplest, and commonly used method [3],[45]-[48]. Other reasons for using this method are a) it tolerances regarding monotonic illumination changes; b) it has ability of describe local image structures; c) it is computationally not expensive; d) it already has many successful face related applications, such as face detection, face recognition, facial expression analysis, demographic (gender, race, age, etc.) classification in recent years [42], several LBP's C/C++ and MATLAB implementations of the can be found online, and finally it used for many different image analysis tasks, such as object image analysis, biomedical image analysis, aerial image analysis, motion analysis, and image and video retrieval. However, a) it cannot capture small 3×3 neighborhood dominant features with large scale structures; b) it is sensitive to a severe illumination (typically during non-monotonic lighting variations) changes; c) it is sensitive to blurred/noisy images; and d) it depends on datasets. Even with big progress in LBP face recognition and several other methods, the accurate face recognition performance is not satisfactory in the presence of illumination changes and occlusions. The

brief surveys on LBP based face analysis with several recent variations are given [51]-[53].

As well, most of face recognition algorithms have been developed for grayscale images but relatively less explored for color cases. The same time, the color information has been proven to be useful in many imaging applications, including the object detection, segmentation, classification and recognition, image retrieval and indexing. Also, color images may be being additional biometric information for face recognition. A few attempts are made to represent color face images in different color spaces, such as YUV, RGB, HSV, YCbCr, YIQ, L*a*b color spaces, or recently developed hybrid color RIQ, RCrQ, RQCr, and CID spaces. It is natural to ask how to combine color and texture features to improve a FR system performance.

The goal of our paper is to propose to gain robust color facial descriptions which reduce the sensitivity of illumination changes, by using a new color image representation and quaternion gradients (used to extract the edges, contours, and texture of faces/objects). In this paper, we propose a novel feature representation based on quaternion gradient-based LBP concept for color face recognition. The rest of the paper is organized as follows. Section 2 presents a novel image representation scheme, while Section 3 introduces the color visibility images. Section 4 proposes a quaternion image gradient concept, and Section 5 presents a new representation of color facial images. Finally, Section 6 contains our conclusions and directions for future research.

Diagram of Facial Image Representation

In this section we briefly describe the grayscale facial image representation, or description, which is based on the local binary patterns (LBP) over the whole facial image [3,5]. We describe this representation in terms of simple gradient operators with following composition of the 8-bit LBP image and its histogram, which can be used as the feature in classification of facial images. The main parts of representation of the grayscale facial image $f_{n,m}$ of size $N \times M$ are shown in the block-diagram of Fig. 1.

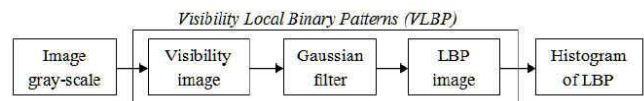


Figure 1. The block-diagram of the facial image representation.

The algorithm of facial image processing can be described by the following steps.

Stage 1. The visibility image is calculated,

$$f_{n,m} \rightarrow V(f)_{n,m}, \quad n = 0:(N-1), m = 0:(M-1).$$

Such an image $V(f)$ can be, for instance, the EME visibility image $E(f)$, which is defined below in Eq. (7). The image $V(f)$ can also be the image obtained by applying one of the gradient operators.

Stage 2. The 2-D Gaussian function is circular convoluted with the visibility image.

$$V(f)_{n,m} \rightarrow V(f)_{n,m} \otimes h_{n,m},$$

where the 2-D Gaussian function

$$h_{n,m} = \frac{1}{K} \exp\left(-\frac{n^2 + m^2}{2\pi\sigma^2}\right)$$

is considered with the mean (0,0) and variance $\sigma^2 = 1/4$. The factor K is calculated by

$$K = \sum_{n=-L_1}^{L_1} \sum_{m=-L_2}^{L_2} h_{n,m} = \sum_{n=-L_1}^{L_1} \sum_{m=-L_2}^{L_2} \exp\left(-\frac{n^2 + m^2}{2\pi\sigma^2}\right).$$

The kernel of the Gaussian function is of size $(2L_1 + 1) \times (2L_2 + 1)$.

Stage 3. A complex gradient image composition is calculated. In the 3×3 -square window W , we consider the following simple set of eight gradient operators:

$$\begin{aligned} A_1 &= \begin{bmatrix} -1 & 0 & 0 \\ 0 & \underline{1} & 0 \\ 0 & 0 & 0 \end{bmatrix}, A_2 = \begin{bmatrix} 0 & -1 & 0 \\ 0 & \underline{1} & 0 \\ 0 & 0 & 0 \end{bmatrix}, A_3 = \begin{bmatrix} 0 & 0 & -1 \\ 0 & \underline{1} & 0 \\ 0 & 0 & 0 \end{bmatrix}, \\ A_4 &= \begin{bmatrix} 0 & 0 & 0 \\ 0 & \underline{1} & -1 \\ 0 & 0 & 0 \end{bmatrix}, A_5 = \begin{bmatrix} 0 & 0 & 0 \\ 0 & \underline{1} & 0 \\ 0 & 0 & -1 \end{bmatrix}, A_6 = \begin{bmatrix} 0 & 0 & 0 \\ 0 & \underline{1} & 0 \\ 0 & -1 & 0 \end{bmatrix}, \\ A_7 &= \begin{bmatrix} 0 & 0 & 0 \\ 0 & \underline{1} & 0 \\ -1 & 0 & 0 \end{bmatrix}, A_8 = \begin{bmatrix} 0 & 0 & 0 \\ -1 & \underline{1} & 0 \\ 0 & 0 & 0 \end{bmatrix}. \end{aligned} \quad (1)$$

The center of the masks is in the original point (0,0) and it is underlined. The order of these gradient operators is shown in Fig. 2.

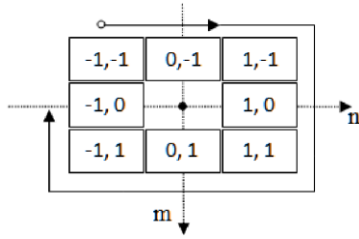


Figure 2. The coordinates and the order of 8 neighbor sampling points.

These eight neighbor points are called the sampling points (SP).

$$SP = [(-1, -1), (0, -1), (1, -1), (1,0), (1,1), (0,1), (-1,1), (-1,0)].$$

The set of sampling points can also be considered in the following order:

$$SP = [(-1, -1), (-1,0), (-1,1), (0, -1), (0,1), (1, -1), (1,0), (1,1)].$$

These gradient operators are applied on the facial image $f_{n,m}$ and eight binary images are calculated by

$$B_k(f)_{n,m} = u[A_k(f)_{n,m}], \quad k = 1:8. \quad (2)$$

Here, $u[t]$ is the Heaviside function that is defined as $u[t] = 1$, if $t \geq 0$, and $u[t] = 0$, otherwise. Then, the new image, which is called the local binary pattern (LBP) image, is calculated by [46,47]

$$b_{n,m} = B_1(f)_{n,m} + 2^1 B_2(f)_{n,m} + 2^2 B_3(f)_{n,m} + \dots + 2^7 B_8(f)_{n,m}. \quad (3)$$

The LBP image can also be written in the standard form

$$b_{n,m} = \sum_{k=1}^8 2^{k-1} [f_{n,m} - f_{n+s(k),m+p(k)}]. \quad (4)$$

Here, $(s(k), p(k))$ are the sampling points, which are ordered as shown in the sampling points SP . The LBP image has the range of 256 integer levels s , from 0 to 255. The histogram of this image, $H(s)$ is considered to

be the feature of the facial image $f_{n,m}$, which can be used in face classification.

As an example, Fig. 3 shows the facial image of size 114×94 in part (a), the EME visibility image in part (b), and the visibility image filtered by the 2-D Gaussian function in part (c).

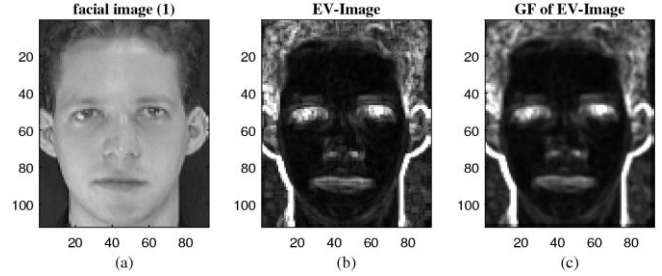


Figure 3. (a) The image and (b) the EME visibility image. (c) The EME visibility image filtered by the 2-D Gaussian function.

Figure 4 shows the LBP image $b_{n,m}$ in part (a) and the histogram of the image in part (b).

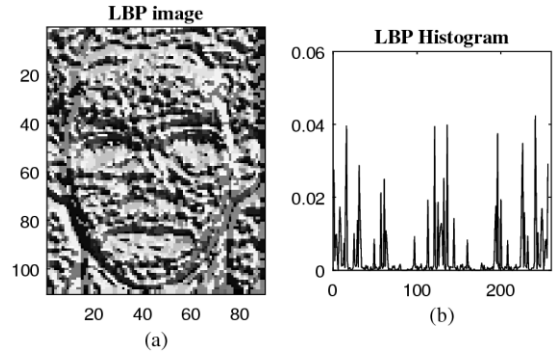


Figure 4. (a) The LBP image and (b) the histogram of the image.

The set of gradients described above are defined by the 3×3 window with the center in the middle. Other gradient operators also can be considered with 3×3 window, as well as with the 5×5 and 7×7 windows, when constructing LBP images with large number of levels.

The histogram of this image has 256 or binary patterns and to reduce the number of binary patterns, the LBP image can be modified, by using a special mapping that is called a uniform LBP look up table (T) and shown below

$$T = \begin{bmatrix} 0 & 1 & 2 & 3 & 4 & 5 & 6 & 7 & \bullet & 8 & \bullet & 9 & 10 \\ 11 & \bullet & \bullet & \bullet & \bullet & \bullet & 12 & \bullet & \bullet & 13 & \bullet & 14 & 15 \\ 16 & \bullet \\ 17 & \bullet & \bullet & \bullet & \bullet & \bullet & 18 & \bullet & \bullet & 19 & \bullet & 20 & 21 \\ 22 & \bullet \\ \bullet & \bullet \\ 23 & \bullet \\ 24 & \bullet & \bullet & \bullet & \bullet & \bullet & 25 & \bullet & \bullet & 26 & \bullet & 27 & 28 \\ 29 & 30 & \bullet & 31 & \bullet & 32 & \bullet & \bullet & \bullet & \bullet & \bullet & \bullet & 33 \\ \bullet & 34 \\ \bullet & \bullet \\ \bullet & 35 \\ 36 & 37 & \bullet & 38 & \bullet & 39 & \bullet & \bullet & \bullet & \bullet & \bullet & \bullet & 40 \\ \bullet & 41 \\ 42 & 43 & \bullet & 44 & \bullet & 45 & \bullet & \bullet & \bullet & \bullet & \bullet & \bullet & 46 \\ 47 & 48 & \bullet & 49 & \bullet & 50 & 51 & 52 & \bullet & 53 & 54 & 55 & 56 & 57 \end{bmatrix}$$

The total number of uniform patterns is 58 and they are labeled from 0 to 57. The label 58 is assigned for all other, non-uniform patterns. By using this table after each gradient image calculation, the new image is calculated as follows:

$$\begin{aligned} (g_1)_{n,m} &= T[(g_1)_{n,m}], \\ (g_k)_{n,m} &= T[(g_{k-1})_{n,m} + B_k(f)_{n,m}], \quad k = 2: 8. \end{aligned} \quad (5')$$

The last image $(g_8)_{n,m}$ has the range of 59 integer levels s , from 0 to 58. The histogram of this image is considered to be the feature of the facial image $f_{n,m}$, which is used in face classification. Thus, 256 integer levels in the original LBP image are reduced to 59 levels in the uniform LBP (ULBP) image.

As an example, Fig. 5 shows the first image $(g_8)_{n,m}$ in part (a) and this image after using the mapping by the ULBP table in part (b). The normalized histogram of the uniform LBP image is given in part (c).

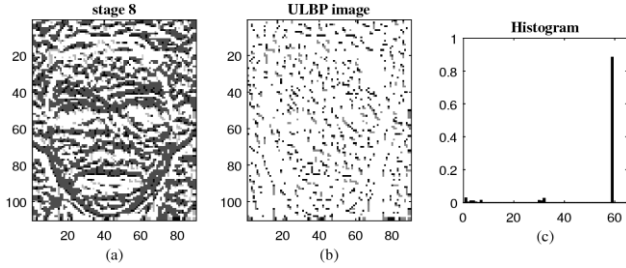


Figure 5. (a) The image $(g_8)_{n,m}$ before the mapping, (b) the uniform LBP image, and (c) the histogram of the image.

Color Visibility Images

The concepts of visibility images can be applied component-wise for color images. We consider the visibility images that are related to the enhancement measure EME [13]-[15], which calculates the average range of intensity of the image in the logarithm scale and the enhancement of the image $f_{n,m}$ is estimated in small not overlapping blocks or windows $W_{k,l}$ of small size. This quantitative measure of the enhanced image, $f_{n,m} \rightarrow g_{n,m}$, is defined by

$$EME(g) = \frac{1}{k_1 k_2} \sum_{k=1}^{k_1} \sum_{l=1}^{k_2} 20 \ln \left[\frac{\max_{W_{k,l}}(g_{n,m})}{\min_{W_{k,l}}(g_{n,m})} \right]. \quad (6)$$

Here, $k_1 k_2$ is the numbers of windows dividing the image, and $\max_{k,l}(g)$ and $\min_{k,l}(g)$ respectively are the maximum and minimum of $g_{n,m}$ inside the window $W_{k,l}$. $EME(g)$ is called a measure of enhancement of the image f . The value of $EME(f)$ is called the enhancement measure of the original image f .

The EME related visibility image at the pixel (n, m) can be defined as follows [43]:

$$E(g)_{n,m} = \ln \left[\frac{\max_W(f_{n,m})}{\min_W(f_{n,m})} \right] (f_{n,m})^\beta, \quad (7)$$

where β is a parameter. If $\min_W(f_{n,m}) = 0$, the value $E(f)_{n,m}$ is considered to be zero. Also, we can add a small number $\varepsilon_0 > 0$ in the denominator in this ratio.

Now, we consider the EME measure and the color image in the RGB model, when image is composed by red, green, and blue components, $f_{n,m} = (r_{n,m}, g_{n,m}, b_{n,m})$. The EME visibility color image (EVCI) is defined by the operator

$$f_{n,m} \rightarrow E(f_{n,m}) = [E(r_{n,m}), E(g_{n,m}), E(b_{n,m})], \quad (8)$$

where the color components of this image are calculated by Eq. 7.

The image $E(f)_{n,m}$ is called the EME visibility image of $f_{n,m}$,

$$E(c_{n,m}) = \ln \left[\frac{\max_W(c_{n,m})}{\min_W(c_{n,m})} \right] (c_{n,m})^\beta. \quad (9)$$

As an example, we consider the color “flowers” image that is shown in Fig. 5 in part (a). The color image composed by the EME visibility images of three color components, calculated with $\beta=1$, is shown in part (b) and the grayscale component of this image in part (c).

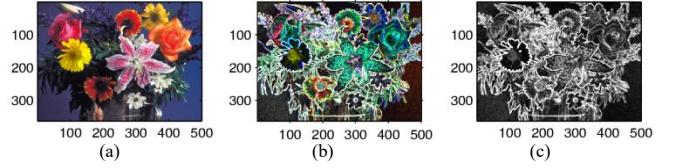


Figure 5. (a) The color “flowers” image, (b) the MEVCI, and (c) grayscale image of the MEVCI.

The visibility images can also be calculated by gradient operators, for instance as

$$E(c_{n,m}) = k \ln \left| \frac{c_{n,m} - \text{mean}_W(c_{n,m})}{c_{n,m} + c_0} \right|. \quad (10)$$

Here, $c_{n,m}$ stands for one of the color components of the image, and c_0 is a small constant, as 0,001, to avoid zeros in the denominator.

The Michelson visibility images are calculated by using the ratios of difference of the local maximum and minimum to their sum at each pixel. The visibility image is defined as [43]

$$E(c)_{n,m} = k \frac{\max_W(c_{n,m}) - \min_W(c_{n,m})}{\max_W(c_{n,m}) + \min_W(c_{n,m})}, \quad (11)$$

where k is a constant.

Figure 6 shows the color “peppers” image in part (a), and the color image composed by the Michelson visibility images (MVI) of three color components in part (b). The grayscale component of the MVCI is shown in part (c).

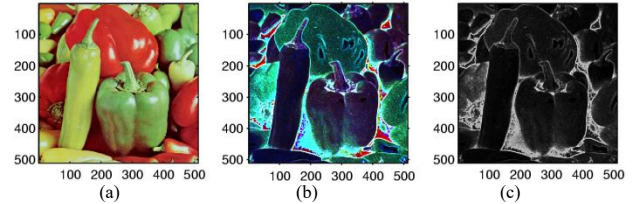


Figure 6. (a) The color “pepper” image, (b) the MVCI, and (c) grayscale image of the MVCI.

Quaternion Image Gradients

The quaternions [31] as doubled complex numbers can be effectively used in processing color image in spatial and complex domains [32]. The three-component imaginary part of the quaternion allows for processing the color as one unit and leads to new approach in image processing, including the enhancement and filtration [33]-[36].

When processing color images, the gradient operators can be defined for color images by operating separately each color component, as well as by introducing new gradient operators in quaternion space wherein color images can be transformed. We describe a few examples of the gradient operators in quaternion imaging. In the RGB model, the $N \times M$ color image $f_{n,m} = (r_{n,m}, g_{n,m}, b_{n,m})$ can be represented in the quaternion space as

$$q_{n,m} = a_{n,m} + (i r_{n,m} + j g_{n,m} + k b_{n,m}). \quad (12)$$

Here, i , j , and k are pure quaternion units, and the real part of the quaternion image is the grayscale image

$$a_{n,m} = (r_{n,m} + g_{n,m} + b_{n,m})/3,$$

or we can consider $a_{n,m} = 0$.

We consider the windowed convolution of this image with a quaternion mask

$$H_{n,m} = (H_e)_{n,m} + (i(H_i)_{n,m} + j(H_j)_{n,m} + k(H_k)_{n,m}),$$

with the right-side multiplication as

$$y_{n,m} = \sum_{n_1=L_1}^{L_1} \sum_{l=L_2}^{L_2} q_{n-n_1, m-m_1} H_{n_1, m_1}$$

where $(2L_1 + 1) \times (2L_2 + 1)$ are size of the mask.

The $H_i, H_j, H_k = 0$ case corresponds to the traditional component-wise color image processing by the real mask by the same real mask H_e . If this mask relates to a gradient operator, we obtain the component-wise edge detection in color imaging. It is clear that not all edges can be found by processing separately the color components by a single gradient.

We consider the cases of most interest, when the kernel is quaternion with the equal components. Thus, let the convolution mask is the quaternion gradient of form

$$H_{n,m} = (1 + (i + j + k))(H_e)_{n,m}, \quad (13)$$

and real mask H_e is defined as for the gradient operator G_x or G_y in the X and Y directions, respectively. Thus, we consider two quaternion gradients

$$H_x = (1 + (i + j + k))G_x$$

and

$$H_y = (1 + (i + j + k))G_y.$$

For example, we consider the 3×3 Sobel gradients with masks

$$G_x = \frac{1}{4} \begin{bmatrix} -1 & 0 & 1 \\ -2 & 0 & 2 \\ -1 & 0 & 1 \end{bmatrix}, \quad G_y = \frac{1}{4} \begin{bmatrix} 1 & 2 & 1 \\ 0 & 0 & 0 \\ -1 & -2 & -1 \end{bmatrix}.$$

The quaternion operators defined with such masks are called the quaternion Sobel gradients [43]. Figure 7 shows the imaginary part of the quaternion H_x -Sobel gradient as a color image is shown in part (a) and the real part of the gradient in part (b).

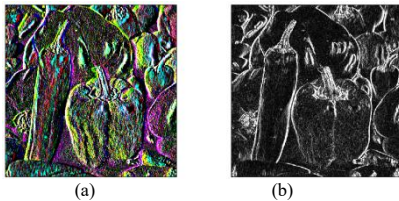


Figure 7. (a) The imaginary part and (b) the real part of the quaternion H_x -Sobel gradient image.

Figure 8 shows the imaginary part of the quaternion H_y -Sobel gradient as a color image is shown in part (a) and the real part of the gradient in (b).

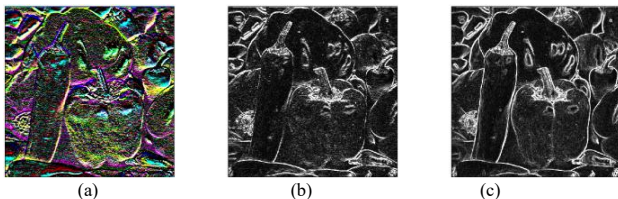


Figure 8. (a) The imaginary part and (b) the real part of the quaternion H_y -Sobel gradient image. (c) The magnitude of the quaternion Sobel gradient image.

Figure 8(c) shows the magnitude of the real part of the quaternion Sobel gradient of the "pepper" image, which is calculated as

$$|[H(q)]_e| = |[H_x(q)]_e| + |[H_y(q)]_e|.$$

The quaternion gradient operators defined with different components $H_i \neq H_j \neq H_k \neq H_e$ can also be considered, when processing the color images in quaternion space. Such gradients can be defined similar to the Prewitt compass quaternion gradient and the Robinson 5-level compass quaternion gradient [43].

Representation of Color Facial Images

The facial color image recognition can be accomplished by analyzing color components separately, or by using the grayscale image calculated as the average of colors in the RGB model [9]. We consider a representation of the color facial image, to obtain a set of features that can be used in face classification, when the color image is transformed into the quaternion space. The color image can be presented as a full quaternion image or as a pure quaternion image, and then can be processed by the quaternion gradient operations, or a visibility image can be calculated. The real component of the obtained quaternion image can be used as a grayscale image for color facial image presentation.

The main parts of processing the color facial image $f_{n,m}$ of size $N \times M$ are shown in the block-diagram of Fig. 9. The color image is considered in the RGB model.

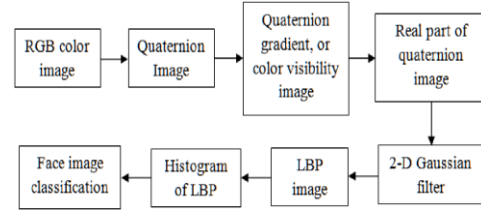


Figure 9. The block-diagram of color facial image processing.

The processing of color images in the XYZ, CMY, CMYK, and other color models is described similar to the RGB model case. The algorithm of the facial image processing can be described by the following steps.

To obtain binary images, the 3×3 -square window W is considered with the eight gradient operators A_1, A_2, \dots, A_8 that are given in Eq. 1. The uniform LBP table is used to compose the new image by applying the uniform LBP table after each gradient image calculation to obtain the images $(g_1)_{n,m}, (g_2)_{n,m}, \dots, (g_7)_{n,m}$, and $(g_8)_{n,m}$, as described in Eq. 5. The histogram of the uniform LBP image, is considered to be the feature of the color facial image, which is used in face classification.

As an example, Fig. 10 shows the color facial image of size 230×266 in part (a). The quaternion gradient image $H(q)_{n,m}$ calculated by using the quaternion gradient in Eq. 13 is shown in part (b), and after filtering by the 2-D Gaussian function with the standard deviation of 0.5 in part (c).

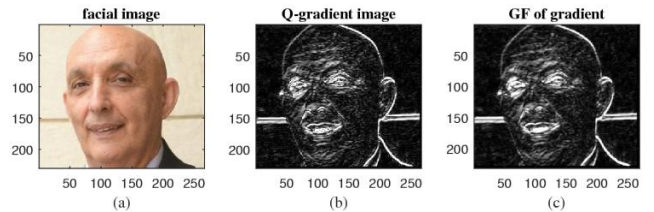


Figure 10. (a) The original image and the quaternion gradient image (b) before and (c) after filtering by the 2-D Gaussian function.

Figure 11 shows the LBP image in part (a) together with its histogram in part (b).

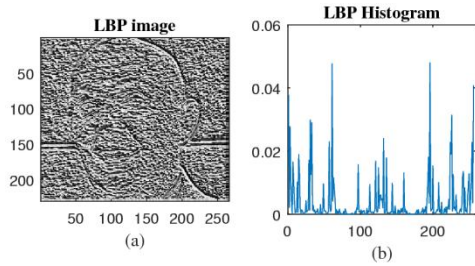


Figure 11. (a) The LBP image and (b) the histogram of this image.

The results of further facial image processing are shown in Fig. 12. The image $(g_8)_{n,m}$ before and after using the mapping by the uniform LBP table is shown in parts (a) and (b), respectively. The normalized histogram of the uniform LBP image is given in part (c).

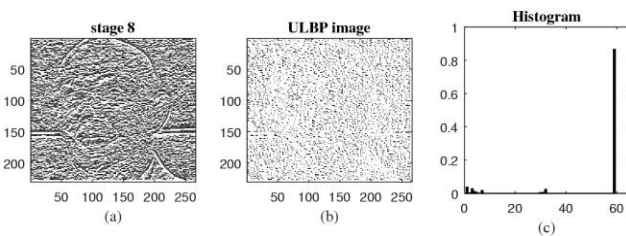


Figure 12. (a) The last binary image $(g_8)_{n,m}$ before the mapping, (b) the uniform LBP image, and (c) the histogram of the image.

We also consider the image from the database designed by Dr. Libor Spacek by address: <http://cswww.essex.ac.uk/mv/allfaces/faces94.html>. Figure 13 shows the 202×182 color facial image “klclar.15.jpg” in part (a). The quaternion gradient image $H(q)_{n,m}$ in part (b) and part (c), after filtering by the 2-D Gaussian function with the standard deviation of 0.5.

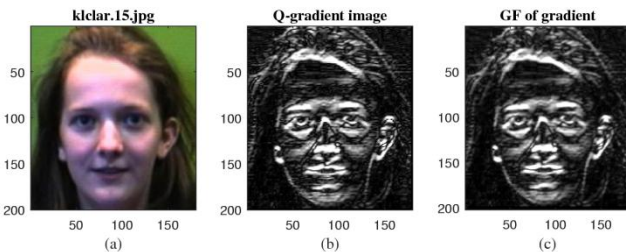


Figure 13. (a) The image and the quaternion Sobel gradient image (b) before and (c) after filtering by the 2-D Gaussian function.

Figure 14 shows the results of further facial image processing. The image $(g_8)_{n,m}$ before and after using the mapping by the uniform LBP table is shown in parts (a) and (b), respectively. The normalized histogram of the uniform LBP image is given in part (c).

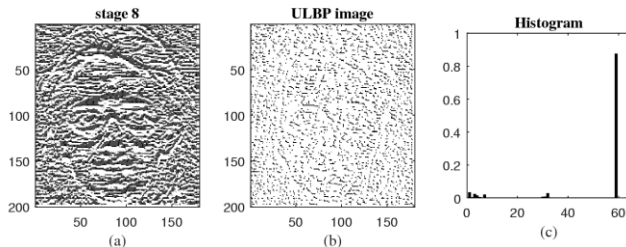


Figure 14. (a) The last binary image $(g_8)_{n,m}$ before the mapping, (b) the uniform LBP image, and (c) the histogram of the image.

We also consider the results of the facial; image processing with the quaternion gradient when 3×3 Prewitt gradients are used with the masks

$$G_x = \frac{1}{5} \begin{bmatrix} 1 & 1 & -1 \\ 1 & -2 & -1 \\ 1 & 1 & -1 \end{bmatrix}, \quad G_y = \frac{1}{5} \begin{bmatrix} 1 & 1 & 1 \\ 1 & -2 & 1 \\ -1 & -1 & -1 \end{bmatrix}.$$

Figure 15 shows the same facial image “klclar.15.jpg” in part (a). The quaternion gradient image $H(q)_{n,m}$ calculated by using the quaternion Prewitt gradient in part (b) and part (c) after filtering by the 2-D Gaussian function with the standard deviation of 0.5.

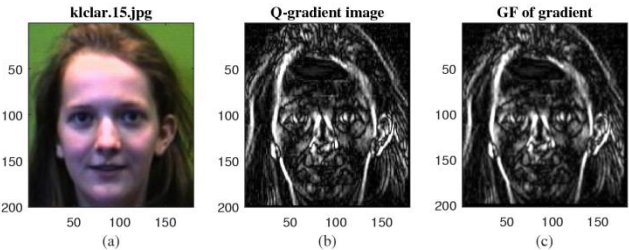


Figure 15. (a) The image and the quaternion Prewitt gradient image (b) before and (c) after filtering by the 2-D Gaussian function.

The image $(g_8)_{n,m}$ before and after using the mapping by the uniform LBP table is shown in Fig. 16 part (a) and (b), respectively. The normalized histogram of the uniform LBP image is given in part (c).

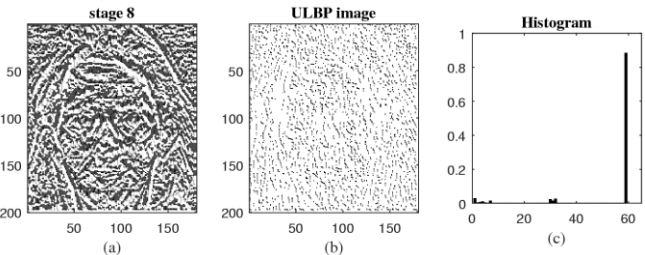


Figure 16. (a) The last binary image $(g_8)_{n,m}$ before the mapping, (b) the uniform LBP image, and (c) the histogram of the image.

Summary

A novel face recognition approach is proposed, by using multiple feature fusion across color, spatial and frequency domains. The proposed approach is useful and applicable not only for face recognition, but also for object recognition. We are planning to evaluate the presented face recognition concept, by using the color FERET database: <http://www.face-rec.org/databases/>.

References

- [1] W. Zhao, R. Chellappa, P. J. Phillips, A. Rosenfeld, “Face recognition: a literature survey,” ACM Computing Survey, vol. 35, pp. 399–458, 2003.
- [2] T. Ojala, M. Pietikäinen, and T. Mäenpää, “Multiresolution gray-scale and rotation invariant texture classification with local binary patterns,” IEEE Trans Pattern Anal Mach Intell., vol. 24, no. 7, pp. 971–987, 2002.
- [3] C. Shan, S. Gong, P.W. McOwan, “Facial expression recognition based on local binary patterns: A comprehensive study,” Image and Vision Computing, vol. 27, pp. 803-816, 2009.

- [4] A. K. Jain, A. Ross, S. Prabhakar, "An introduction to biometric recognition," *IEEE Trans. Circuits Syst. Video Technol.*, vol. 14, no. 1, pp. 4–20, 2004.
- [5] T. Ahonen, A. Hadid, M. Pietikainen, "Face description with local binary patterns: Application to face recognition," *IEEE Trans. Pattern Anal. Mach. Intell.*, vol. 28, no. 12, pp. 2037–2041, 2006.
- [6] L. Wolf, T. Hassner, T. Taigman, "Effective unconstrained face recognition by combining multiple descriptors and learned background statistics," *IEEE Trans. Pattern Anal. Mach. Intell.*, vol. 33, no. 10, pp. 1978–1990, 2011.
- [7] J. Mennesson, C. Saint-Jean, L. Mascarilla, "New geometric Fourier descriptors for color image recognition," in *IEEE International Conference on Image Processing (ICIP)*, 2010, pp. 2685–2688.
- [8] S. Nikan, M. Ahmadi, "Partial face recognition based on template matching," *Proc. 11th International Conference on Signal-Image Technology & Internet-Based Systems*, p. 160-163, 2015.
- [9] H. Tang, B. Yin, Y. Sun, and Y. Hu, "3D face recognition using local binary patterns," *Signal Process.*, vol. 93, pp. 2190-2198, 2013.
- [10] B.K.P. Horn, *Robot Vision*, The MIT Press, Cambridge, 1986.
- [11] W.K. Pratt, *Digital Image Processing*, 3rd Edition, John Wiley & Sons, Inc., 2001.
- [12] R.C. Gonzalez, R.E. Woods, *Digital Image Processing*, 2nd Edition, Prentice Hall, Upper Saddle River, New Jersey, 2002.
- [13] S.S. Agaian, K. Panetta, A.M. Grigoryan, "A new measure of image enhancement," *Proc. IASTED Int. Conf. Signal Processing & Communication*, Marbella, Spain, pp. 19–22, 2000.
- [14] S.S. Agaian, K. Panetta, A.M. Grigoryan, "Transform-based image enhancement algorithms," *IEEE Trans. on Image Processing*, vol. 10, no. 3, pp. 367–382, 2001.
- [15] A.M. Grigoryan, S.S. Agaian, *Multidimensional Discrete Unitary Transforms: Representation, Partitioning and Algorithms*, Marcel Dekker Inc., New York, 2003.
- [16] Z. Rahman, D. Jobson, G.A. Woodell, "Retinex processing for automatic image enhancement," *Journal of Electronic Imaging*, vol. 13, no. 1, pp. 100-110, 2004.
- [17] A.M. Grigoryan and S.S. Agaian, "Adapted Retinex Algorithm with Complexity Optimization for Mobile Phone Medical Image Enhancement," - chapter 5, pp. 119-151. In *Electronic Imaging Applications in Mobile Healthcare*, J. Tang, S.S. Agaian, and J. Tan, Eds., SPIE Press, Bellingham, Washington, February 2016,
- [18] F.T. Arslan, A.M. Grigoryan, "Fast splitting alpha-rooting method of image enhancement: Tensor representation," *IEEE Trans. on Image Processing*, vol. 15, no. 11, pp. 3375–3384, 2006.
- [19] A.M. Grigoryan, S.S. Agaian, "Monotonic sequences for image enhancement and segmentation," *Digital Signal Processing*, vol. 41, pp. 70–89, 2015, (doi:10.1016/j.dsp.2015.02.011)
- [20] A.M. Grigoryan, S.S. Agaian, "Preprocessing Tools for Computer-Aided Cancer Imaging Systems," in "Computer-Aided Cancer Detection and Diagnosis: Recent Advances" (Editors: J. Tang and S. Agaian), SPIE, chapter 2, p. 55, 2014.
- [21] A.M. Grigoryan, S.S. Agaian, "Transform-based image enhancement algorithms with performance measure," *Advances in Imaging and Electron Physics*, Academic Press, vol. 130, pp. 165–242, 2004.
- [22] A.M. Grigoryan, M.M. Grigoryan, *Brief Notes in Advanced DSP: Fourier Analysis With MATLAB*, CRC Press, Taylor and Francis Group, Boca Raton, New York, 2009.
- [23] W.M. Morrow, R.B. Paranjape, R.M. Rangayyan, J.E.L. Desautels, "Region based contrast enhancement of mammograms," *IEEE Trans. on Medical Imaging*, vol. 11, no. 3, pp. 392–406, 1992.
- [24] P. Zamperoni, "Image enhancement," *Advanced in Image and Electron Physics*, vol. 92, pp. 1–77, 1995.
- [25] E.A. Silva, K.A. Panetta, S.S. Agaian, "Quantify similarity with measurement of enhancement by entropy," *Proc. SPIE*, vol. 6579, 65790U, 2007.
- [26] K.A. Panetta, E.J. Wharton, S.S. Agaian, "Human visual system-based image enhancement and logarithmic contrast measure," *IEEE Transactions on Systems, Man, and Cybernetics, Part B (Cybernetics)*, vol. 38, no. 1, pp. 174–188, 2008.
- [27] E. Wharton, S. Agaian, K. Panetta, "A logarithmic measure of image enhancement," *Proc. SPIE*, vol. 6250, 62500P, 2006.
- [28] E. Wharton, K. Panetta, S. Agaian, "Human visual system based similarity," *Proc. Systems, Man and Cybernetics, SMC 2008. IEEE International Conference on*, pp. 685–690, 2008.
- [29] S. Agaian, "Visual morphology," *Proc. SPIE*, 3646, 1999.
- [30] K.A. Panetta, C. Gao, S.S. Agaian, "No reference color image contrast and quality measures," *IEEE Transactions on Consumer Electronics*, vol. 59, no. 3, pp. 643–651, 2013.
- [31] W.R. Hamilton, *Elements of Quaternions*, Logmans, Green and Co., London, 1866.
- [32] A.M. Grigoryan, S.S. Agaian, "Retolling of color imaging in the quaternion algebra," *Applied Mathematics and Sciences: An International Journal (MathSJ)*, vol. 1, no. 3, pp. 23–39, 2014.
- [33] A.M. Grigoryan, J. Jenkinson, S.S. Agaian, "Quaternion Fourier transform based alpha-rooting method for color image measurement and enhancement," *SIGPRO-D-14-01083R1*, *Signal Processing*, vol. 109, pp. 269–289, April 2015, (doi:10.1016/j.sigpro.2014.11.019)
- [34] A.M. Grigoryan, S.S. Agaian, "Alpha-rooting method of color image enhancement by discrete quaternion Fourier transform," *Proc. SPIE*, vol. 9019, 901904, 2014.
- [35] A.M. Grigoryan, J. Jenkinson, S.S. Agaian, "Quaternion Fourier transform based alpha-rooting method for color image measurement and enhancement," *SIGPRO-D-14-01083R1*, *Signal Processing*, vol. 109, pp. 269–289, 2015.
- [36] A.M. Grigoryan, S.S. Agaian, "Color Enhancement and Correction for Camera Cell Phone Medical Images Using Quaternion Tools," Chapter 4, pp. 77–117. In book: *Electronic Imaging Applications in Mobile Healthcare*, (J. Tang, S.S. Agaian, and J. Tan, Eds.) SPIE Press, Bellingham, Washington, 2016.
- [37] S.C. Necessian, S.S. Agaian, K.A. Panetta, "Multi-scale image enhancement using a second derivative-like measure of contrast," *Proc. SPIE*, vol. 8295, 82950Q, 2012.
- [38] R. Kogan, S. Agaian, K.A. Panetta, "Visualization using rational morphology and zonal magnitude reduction," *Proc. SPIE*, vol. 3304, 1998.
- [39] E. Wharton, S. Agaian, K. Panetta, "Adaptive multi-histogram equalization using human vision thresholding," *SPIE Electronic Imaging*, 2007.

- [40] K. Panetta, L. Bao, S. Agaian, "A human visual "no-reference image quality measure," IEEE Instrumentation & Measurement Magazine, vol. 19, no. 3, pp. 34–38, 2016.
- [41] C. Gao, K. Panetta, S. Agaian, "Color image attribute and quality measurements," Proc. SPIE, vol. 9120, 91200T, 2014.
- [42] C. Gao, K. Panetta, S. Agaian, "No reference color image quality measures," Cybernetics (CYBCONF), 2013 IEEE International Conference on, pp. 243–248, 2013.
- [43] A.M. Grigoryan, S.S. Agaian, Practical Quaternion Imaging With MATLAB, SPIE PRESS, 2018.
- [44] P.J. Phillips, H. Moon, S. Rizvi, P. Rauss, "The FERET evaluation methodology for face recognition algorithms," IEEE Trans. Pattern Analysis and Machine Intelligence, vol. 22, no. 10, pp. 1090-1104, 2000.
- [45] Zhang C., Zhang Z., 2010. "A Survey of Recent Advances in Face Detection," Microsoft Research Technical Report, MSR-TR-2010-66.
- [46] Di Huang, C. Shan, M. Ardebilian, Y. Wang, L. Chen, "Local binary patterns and its application to facial image analysis: A Survey," <http://iris.cnrs.fr/Documents/Liris-5004.pdf>
- [47] "Color local phase quantization (CLPQ)- A new face representation approach using color texture cues," https://www.researchgate.net/publication/303408899_Color_Local_Phase_Quantization_CLPQ-A_New_Face_Representation_Approach_using_Color_Texture_Cues, 2018.

Author Biography

Artyom Grigoryan received the MS degrees in mathematics from Yerevan State University (1978), in imaging science from Moscow Institute of Physics and Technology (1980), and in electrical engineering from Texas A&M University (1999), and PhD degree in mathematics and physics from Yerevan State University (1990). He is an associate professor of the ECE Department, College of Engineering, University of Texas at San Antonio. He is author of 4 books, 10 book-chapters, 3 patents, 120 papers.

Sos Agaian received the M.S. degree in mathematics and mechanics from Yerevan University, Armenia, the Ph.D. degrees in math and physics from Steklov Institute of Mathematics, Russian Academy of Sciences, and in engineering from Institute of Control System, Russian Academy of Sciences. He is professor of the Science Department, College of Staten Island. He is Fellow of the SPIE, IEEE, AAAS, and IS&T. He has authored of 500 scientific papers, 7 books, holds 14 patents.